Optical Properties of Natural $In_xGa_{1-x}As$ Quantum Dots Grown on High-Index GaAs Substrates

P. P. González-Borrero*, D. I. Lubyshev, E. Petitprez,
N. La Scala Jr., E. Marega Jr. and P. Basmaji
Instituto de Física de São Carlos, Universidade de São Paulo,
CP 369, CEP 13560-970 São Carlos, São Paulo, Brazil

Received November 11, 1996

In this work optical properties of $In_xGa_{1-x}As$ quantum dots (QDs) grown by molecular bearn epitaxy are investigated. The quantum dots were grown on GaAs reference (001) and on (n11)A/B (where n = 1, 2, 3, 5 and 7) substrates. They were characterized by photoluminescence (PL) measurements. The results show a high crystal quality of quantum dots grown on (n11)B surfaces based on a strong integrated PL intensity. Temperature dependence indicates an additional lateral confinement on surfaces where QDs are formed. We also observed an unusual decrease of PL peak full width at half maximum with temperature, suggesting suppression of non-predominant size QD emissions due to carrier tunneling between nearby dots. Optical properties of vertically self-organized quantum dot islands were also examined via PL spectroscopy. The experimental results show a dependence of PL emission on substrate orientation and spacer layer thickness.

I. Introduction

Three-dimensional (3D) carrier quantum confinement makes semiconductor quantum dots (QDs) a unique system in which are expected a strong increase in exciton binding energy and oscillator strength[1,2] as well as improvement in laser performance[3−6]. Therefore, the fabrication of quantum dots is important not only for basic physics but also for optoelectronic device applications[1]. In order to form such systems several approaches have been carried out. The earliest one is based upon growth on non-planar patterned substrates[7] and, later, growth on planar masked substrates[8] and on planar high-index surfaces that provide a natural structural corrugation[9]. These three classes of substrates have a controlled starting surface pattern. In contrast, for high lattice mismatched systems, the strain induced 3D coherent islands formed on planar substrates could potentially serve as QDs. Among these growth methods, the latest (based on Stranski-Krastanov growth mode) could be a promising path for the creation of damage free dot structures directly on the epilayer surface[10−13]. This growth method begins with an initial two-dimensional (2D) deposition on the substrate material. After a critical thickness is achieved, the surface is transformed into highly strained 3D islands that grow coherently on the heterostructure interface. The great advantage of this dot (island) fabrication technique is that no nanolithography or etching process are needed, avoiding dislocation and defect creation at QD interfaces. This technique also allows high dot density (up to $\sim 10^{11}$ cm^{-2}) to be reached[14].

Most of the research is currently conducted by molecular beam epitaxy (MBE)[14,15] or metalorganic chemical vapor deposition (MoCVD)[16,17] on GaAs(001) substrates. Few studies on QD formation on GaAs high-index surfaces have been reported[16,17]. It has been suggested by Sangter[18] that (n11) surfaces present a high density of steps compared to the atomically flat (001) surface. Grunthaner et al.[19] have in-

*Corresponding author: Email: Gonzalez@ifqsc.sc.usp.br; Fax: + 55 16 2713616

dicated that the critical thickness, reached before an island morphology generation, is strongly dependent on this step density. During MBE growth these high-index planes break up into periodic arrays of nanometer scale facets, lowering the surface energy. This microscopic surface morphology represents equilibrium surface structure, and is generally stable during growth. Therefore, the lateral periodicity is fixed for a certain crystallographic orientation[9,20]. Such periodicity might influence the adatom kinetic, resulting in different stress relaxation for each surface, which gives rise to differences in dot shape and defect density at dot interfaces, influencing optical recombination efficiency. These conditions determine growth mode for each orientation.

In this paper we report and summarize results of the study of $In_xGa_{1-x}As$ (with $x = 1.0$ and $x = 0.5$) QD formation, using the Stranski-Krastanov growth mode. These QDs were produced by MBE technique, growing the structure on GaAs(n11)A/B and on reference (001) substrates. The study is mainly based on the optical properties of such structures since, for QD application in optoelectronic devices, a detailed characterization of photoluminescence (PL) properties is fundamental. PL measurements were systematically carried out as a function of temperature, excitation power and polarization. The measurements confirm that the naturally formed islands exhibit quantum-effect properties and that PL properties of quantum dots depend on the crystallographic orientation. We will also present preliminary results of optical properties on vertically self-organized InGaAs quantum dot islands as a function of substrate orientation and spacer layer thickness.

II. Growth of quantum dots

The samples were grown by the MBE technique, using a MECA 2000 system, on GaAs reference (001) and (n11)A/B (where n is 1, 2, 3, 5 and 7) substrates (GaAs growth rate of 1 μm/h). Growth process was monitored *in situ* by a reflection high-energy diffraction (RHEED) system operated at 15 kV. The structure basically consists in 20 periods of GaAs/AlAs (2nm/2nm) superlattice, a 0.5 μm GaAs buffer layer, and a 3 nm $In_{0.2}Ga_{0.8}As$ quantum well (QW). The quantum dots were separated from the QW by a 100 nm GaAs layer (see Fig. 1). Growth conditions are summarized in Table 1. Further details about growth of natural QDs are described elsewhere[21,22]. Growth rates were determined by RHEED oscillation technique on the GaAs(001) plane. Since the QD growth temperature was below critical temperature for starting indium re-evaporation, we assume these rates to be the same for all orientations. Interface smoothness was carried out, using growth interruption, before and after InAs and $In_{0.5}Ga_{0.5}As$ deposition (see Table 1). QD nucleation was observed directly by RHEED on (001) surface, when the pattern changed from streaky to spotty.

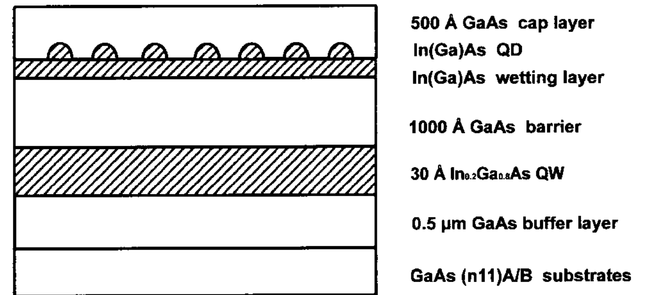

Figure 1. Schematic drawing of the grown structure.

Table 1. Growth conditions for QD formation.

Growth parameter	InAs	$In_{0.5}Ga_{0.5}As$
Growth temperature	500 °C	520 °C
Growth interruption		
- before	1 min	1 min
- after	3 min	3 min
Growth rate	0.061 nm/s	0.11 nm/s
As_4 background pressure	9 x 10 $^{-6}$ Pa	9 x 10 $^{-6}$ Pa
number of monolayer	6 ML	15 ML

III. Photoluminescence measurements and discussions

For PL experiments the samples were mounted in a closed-cycle He cryostat and excited by the green line (514.5 nm) of an Ar^+ laser. The average excitation density was 150 W/cm^2. Emitted light was focused on the entrance slit of a 0.5 m single-grating monochromator and analyzed by a photomultiplier using a detection system in lock-in mode.

III.1 PL intensity at constant temperature

Fig. 2 shows low temperature normalized PL spectra (dotted lines) for $In_{0.5}Ga_{0.5}As$ QDs. Two main features are visible for each orientation associated with a QD and a QW PL peak. The observed QD luminescence around 1.27 eV for (001) plane is in agreement with the value reported in Ref. [23]. However, wetting layer peak was not detected in these samples. We suppose this to be related to growth interruption before the cap layer, driving much of the deposited indium to island nucleation, leaving a thin wetting layer. In this case, carriers generated in the wetting layer transfer quickly ($\sim$ ps) to InGaAs islands where they recombine radiatively.

Regarding just the QW peak position, we observed a redshift for the high-index plane samples (see Table 2). Fig. 2 makes clear that the peak position depends on crystallographic orientation. From (001) to (311)A/B surfaces, a decrease is observed in the QW PL peak position and, reversely from (311)A/B to (111)A/B planes, an increase. We believe that this behavior is mainly related with interface roughness as well as, in minor degree, with indium segregation due to surface step density[22]. QWs grown on (n11)A surfaces exhibit a smaller full width at half-maximum (FWHM) when compared with the (n11)B planes (see Table 2). We suppose this characteristic is also related with surface step density structure since (n11)A-orientations are expected to minimize the incorporation of impurities and defects due to empty dangling bonds of their step-edge group III atoms[24].

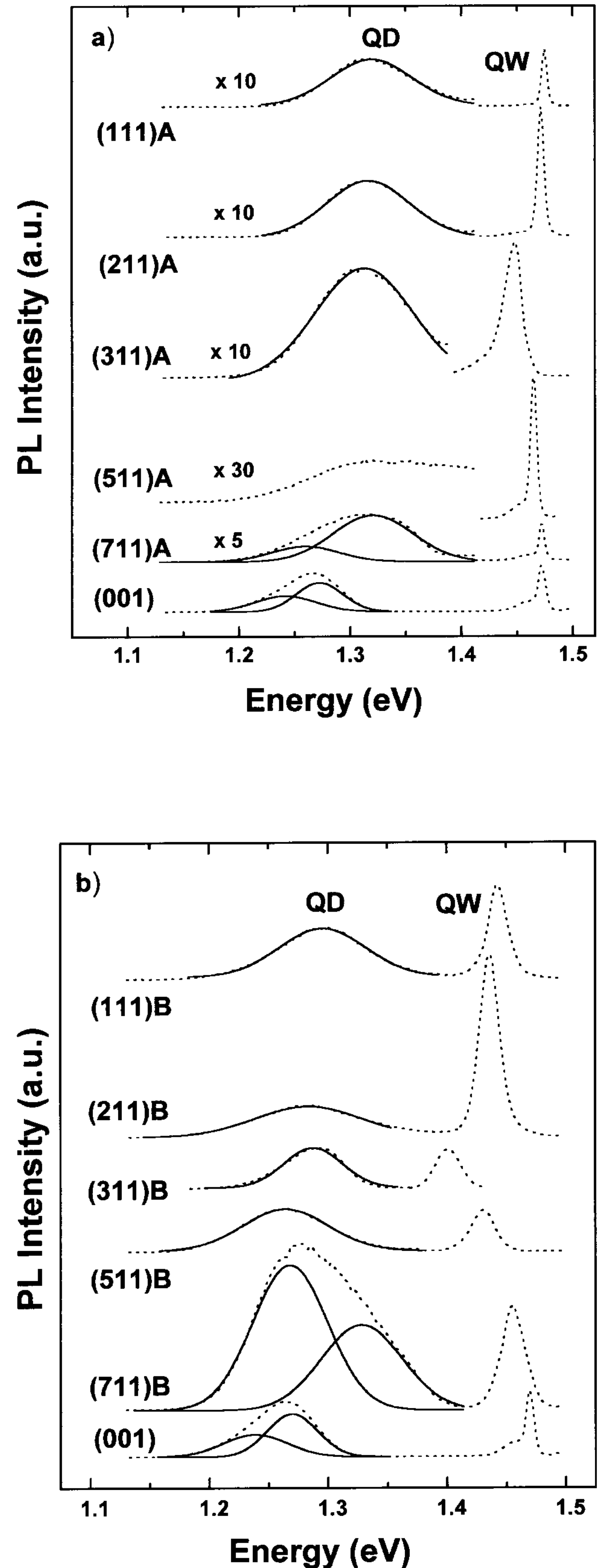

Figure 2. Normalized PL spectra of self-assembled InGaAs QDs grown on high-index (a) (n11)A-GaAs and (b) (n11)B-GaAs surfaces (dotted lines) and Gaussian fitting for QDs (solid lines). (Taken from Ref. [22].)

Table 2.

QW shift energy ΔE_{QW} (= $E_{QW\,(100)}$ - $E_{QW\,(n11)}$) in meV, FWHM values (in meV) for InGaAs-QWs and -QDs on all orientations, and ratio between QD and QW integrated intensity IPL. $E_{QW(100)}$ = 1.470 eV.

Orientation	FWHM		ΔE_{QW}	IPL
	QW	QD		
(100)	7.7	64	-	5.9
(711)A	6.1	103	0	2.6
(711)B	22.1	108	13	10.5
(511)A	6.4	-	7	-
(511)B	23.6	80	39	3.2
(311)A	19.2	98	24	0.2
(311)B	23.6	55	68	3.5
(211)A	6.8	83	0	0.3
(211)B	19.2	96	33	0.9
(111)A	4.6	83	-3	0.5
(111)B	19.2	85	26	2.4

Another interesting feature in Fig. 2 relates to the 2D PL signals. Peak positions, FWHM and the integral luminescence ratio QD/QW values for all samples are listed in Table 2. QDs grown on nonequivalently oriented substrates present significant differences. When the orientation changes from (001) to (111)A/B, a blue shift in QD PL peak is observed. In addition, we noticed that most of the QD peaks (dotted lines) can be fitted by one Gaussian curve (solid lines). In the case of the (001) and (711)A/B oriented surfaces, the fitting requires two Gaussian components that remain stable when excitation density is increased[22]. For the (511)A plane, QD PL signal detection was not possible. QDs grown on (n11)A orientations frequently show smaller FWHM than those grown on (n11)B surfaces, evidencing their superior uniformity. This homogeneity in size was found to be superior on the (311)B surface, revealing a higher degree of ordering as compared to other orientations. This result is in agreement with QD size homogeneity on (311)B plane obtained by MOCVD[16,17]. Table 2 reveals that, for (n11)A surfaces, QD integrated PL intensity is smaller than in QW, except for (711)A plane, whose value is two times larger than the QW's. Besides, the strong integrated PL intensity of QDs grown on (n11)B orientations shows the higher quality of dot interface. This intensity is comparable to that of QW, and for (711)B plane the value is one order of magnitude larger at low temperature (see Table 2). The ratio between QD and QW intensities increases at higher temperatures, a characteristic whose origen will be discussed in the next section. Evidence of QD's defect-free nature can be revealed in an efficient PL signal (mainly for the (n11)B surfaces (see Fig. 2b)), as well as in the linear reponse of the integrated emission intensity with laser excitation density in a range of 10-10^3 W/cm^2 [22].

Fig. 3 shows PL spectra for InAs QD at 16K for some orientations. Concerning the reference quantum well position, we have also observed that PL peak position and PL FWHM depend on crystallographic orientation as noted above for InGaAs QDs. Such an effect has already been reported in Ref. [22]. For (001), (n11)B, (211)A and (111)A surfaces, an additional peak has been detected around 1.35 meV and is attributed to quantum dot formation on each orientation. High QD PL efficiency was obtained for (001) and (711)B surfaces, where QD-QW wavelength-integrated PL intensity ratio is 3.2 and 1.9, respectively. In the other planes, this ratio was one order of magnitude smaller. Peak positions, FWHM, and the integral luminescence ratios QD/QW for InAs QD samples are listed in Table 3. For each orientation, the QD peak was fitted by one Gaussian line. In the case of (511)B plane, the fitting shows a high-energy peak that we attribute to the contribution of wetting layer to the PL signal. In Fig. 3a, each spectrum shows an unlabeled peak around 1.43 eV. Taking into account well width (3 nm) and indium content (20%), as well as temperature dependence of both unlabeled peak position and its intensity, and power density dependence, we can ascribe it to a wetting layer signal. For (001) and (711)B surfaces, this signal was not detected due to high PL efficiency of QDs.

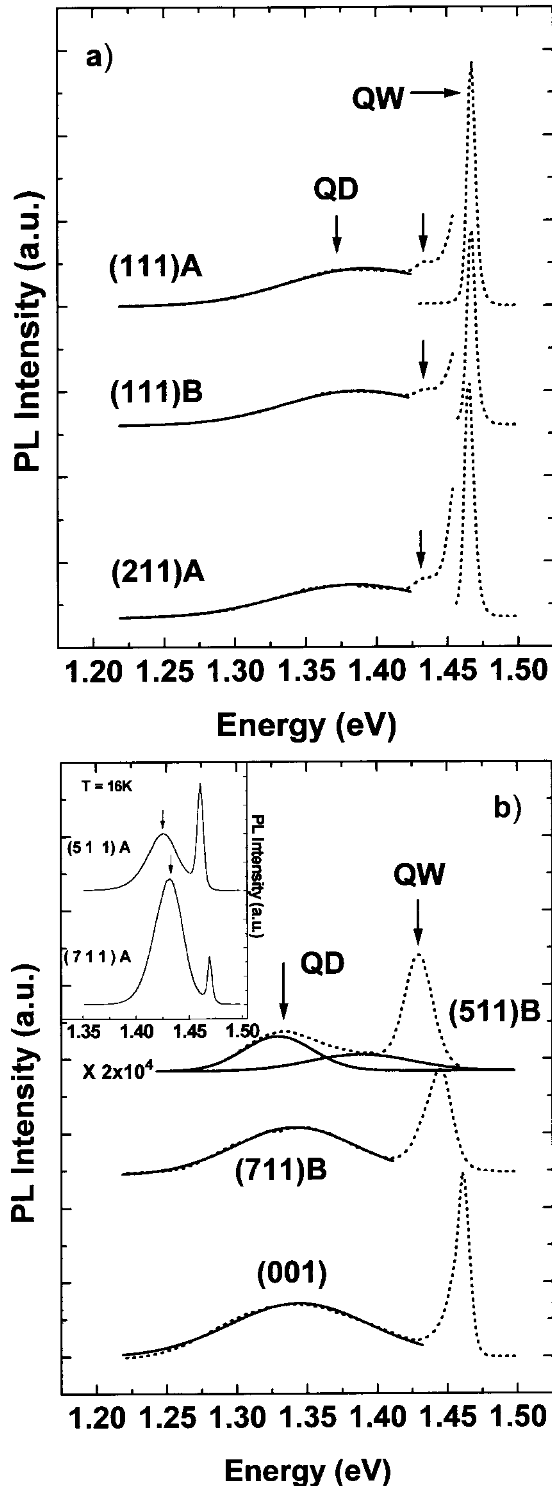

Figure 3. PL spectra of self-organized InAs QDs grown on high-index (a) (211)A, (111)A/B GaAs and (b) (001), (711)B and (511)B GaAs surfaces (dotted lines) and Gaussian fitting for QDs (solid lines). The inset to Fig. 3(b) shows the PL spectra for (511)A and (711)A surfaces, where the grown structure does not exhibit QD formation. The unlabeled peaks were attributed to the wetting layer PL signal. (Taken from Ref. [25]).

Table 3. Peak energy (in eV), FWHM (in meV), and QD-QW wavelength-integrated PL (IPL) intensity ratio for InAs QDs.

	Quantum	Dot	Quantum	Well	
Orientation	E_P	FWHM	E_P	FWHM	IPL
(001)	1.338	123	1.461	12	3.2
(711)B	1.344	102	1.444	~23	1.9
(511)B	1.330	58	1.430	24	0.1
(211)A	1.381	128	1.466	7	0.1
(111)A	1.392	136	1.468	6	0.1
(111)B	1.387	132	1.468	6	0.2

The inset of Fig. 3b exhibits PL spectra for (511)A and (711)A planes[25]. The arrows indicate an additional structure, whose energy position is higher than the QD. We believe this PL feature to be related to a two- dimensional layer (QW) formed after stress relaxation of a critical InAs layer. Enhancement of the FWHM of this PL signal, observed in comparison to reference QW, is probably due to the formation of dislocations or related defects as a result of stress relaxation. Non-QD formation on (511)A has been previously reported[17,22]

III.2 PL temperature dependence

In order to obtain additional information about QD properties, measurements of PL temperature dependence were performed. The particular cases of (711)B and (511)B PL spectra for $In_{0.5}Ga_{0.5}As$ and InAs QD respectively are shown in Fig. 4. This dependence shows a persistence of QD PL signal at high temperature (130 K), while QW PL intensity decreases drastically when temperature changes from 16 K to 70 K. Such persistence at high temperatures is related to the increase of oscillator strength due to additional lateral confinement. The Fig. 4b inset shows PL temperature dependence for (511)A surface. Behavior of the additional structure, indicated by arrows, obviously differs from (511)B QD, a characteristic also suggesting the

existence of stress-related defects, and apparent lack of relation between this peak and QD formation.

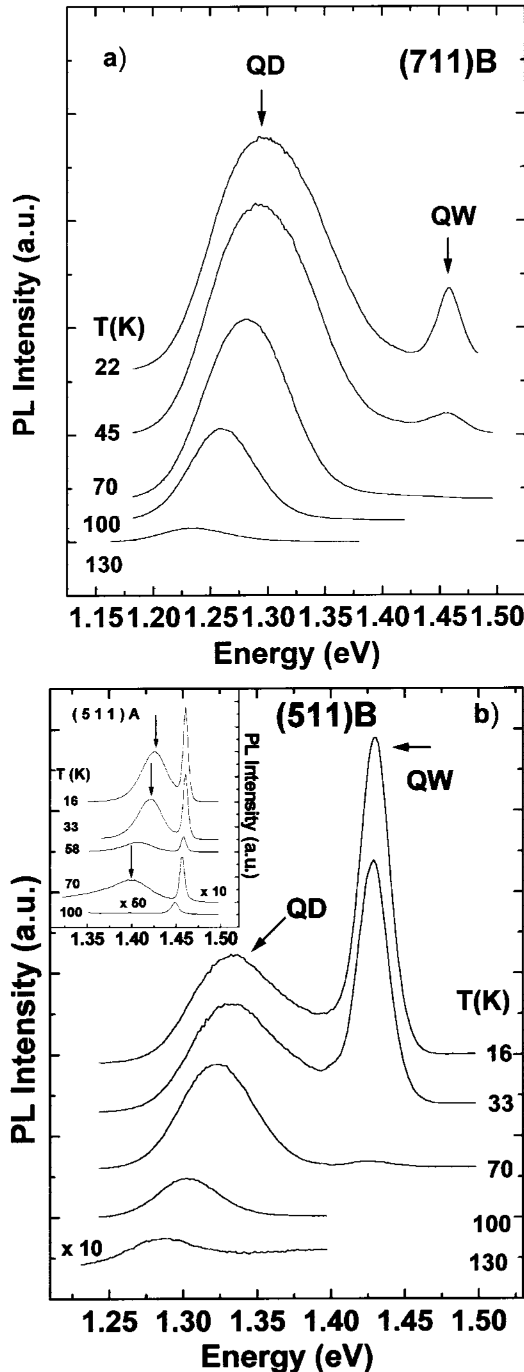

Figure 4. PL temperature dependence of (a) InGaAs QDs grown on (711)B and (b) InAs QDs grown on (511)B and (511)A (inset). The arrow in the inset indicates the presence of an unexpected peak (see text). (Taken from Ref [22] and [25].)

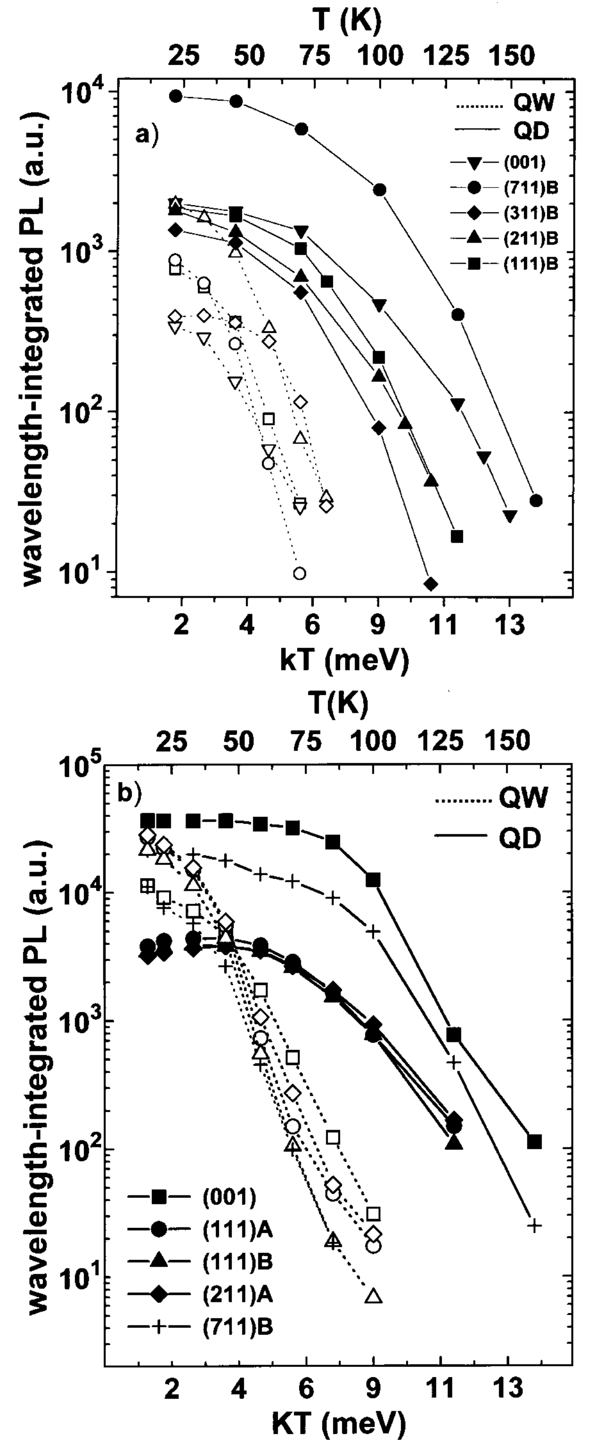

Figure 5. Wavelength-integrated QW (open symbols) and QD (closed symbols) PL temperature dependence of (a) InGaAs- and (b) InAs-QDs for some orientations. (Taken from Ref. [25] and [28].)

Wavelength-integrated PL intensity temperature dependence has also been computed for the cases of QWs and QDs (see Fig. 5). For all orientations, QD PL intensity presents a lesser decrease than QW's at higher temperature, as emphasized earlier. From these plots were extracted the values for thermal quenching

energy (E_Q), averaging 3 and 2.5 times smaller for QWs than for InAs and InGaAs QDs, respectively. Activation energy values for electron-hole emission (E_A) were determined through Arrhenius plots. Tables 4 and 5 show E_Q- and E_A-values for some orientations. E_A values observed for InAs and InGaAs QDs are respectively about 1.4 to 2.4 times and 2 to 5 times larger than for QW, evidencing a lesser suppression of electron-hole emission from QDs compared to QW PL emission, due to an increase in the binding energy.

Table 4. Thermal quenching energy (E_Q) and electron-hole emission activation energy (E_A) values in meV for InGaAs-QDs.

Orientation	E_Q-QW	E_Q-QD	E_A-QW	E_A-QD
(100)	2	5	24	135
(711)B	2	5	46	159
(311)B	4	4	31	50
(211)B	2	3	44	78
(111)B	2	5	35	96

Table 5. Thermal quenching energy (E_Q) and electron-hole emission activation energy (E_A) values in meV for InAs QDs.

Orientation	E_Q-QD	E_Q-QW	E_A-QD	E_A-QW
(001)	6	2	47	24
(711)B	4	1.5	52	22
(511)B	6	2	40	28
(211)A	6	2	28	20
(111)A	6	2	27	19
(111)B	6	2	32	23

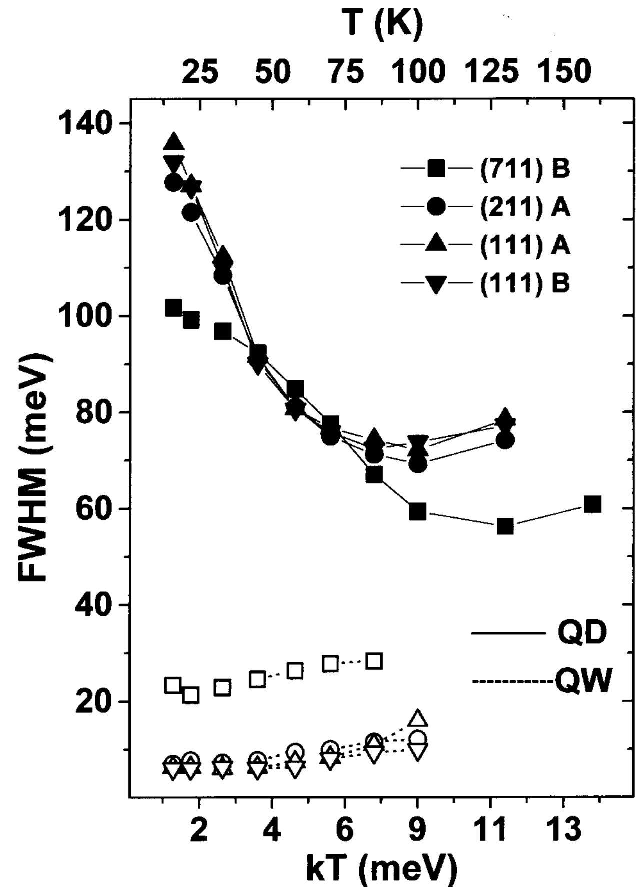

Figure 6. QD (closed symbols) and QW (open symbols) PL FWHM temperature dependence. (Taken from Ref. [33].)

A remarkable effect reported, for the first time as far as we know in Ref. [21] is in the behavior of PL FWHM as a function of temperature. Fig. 6 shows this phenomenon for InAs QDs. An anomalous decrease of QDs PL FWHM was detected for Gaussian-shaped emission from 22 K to ~130 K. This effect has been described in terms of the suppression of non-predominant size QD emissions and the persistence of predominant size ones, contributing to the center of Gaussian shaped PL curve[21], a phenomenon also recently reported for InAs QDs in Ref. [26]. The cited authors proposed a model, involving exciton recombination, thermal activation and transfer. This model does not completely describe our experimental data as to the way that the Gaussian shape of QD PL peak is maintained as temperature rises[21]. In the InGaAs QD case, this effect was not always observed in our samples when the amount of InGaAs was varied. Furthermore, its decrease in the PL FWHM was not as pronounced as in InAs QDs.

III.3 PL polarization dependence

QD PL polarization dependence measurements were also carried out to determine the most probable structural anisotropy of QDs in-plane. To eliminate polarization effects of the experimental setup in our system, unpolarized white light was used. The angular dependence of normalized PL peak intensity for QDs grown on different orientations is shown in Fig. 7, evidencing a strong polarization effect. A maximum of PL intensity was set for PL component with polarization angle zero, occurring when polarization is parallel to the following crystallographic directions: $[1\bar{1}0]$ for (001) plane, $[\bar{2}77]$ for (711), $[\bar{2}55]$ for (511), $[\bar{2}33]$ for (311), $[\bar{1}11]$ for (211) and $[\bar{2}11]$ for (111), respectively. Based on our results, we believe that QDs grown on these planes have well-developed microfacet configuration[27−29].

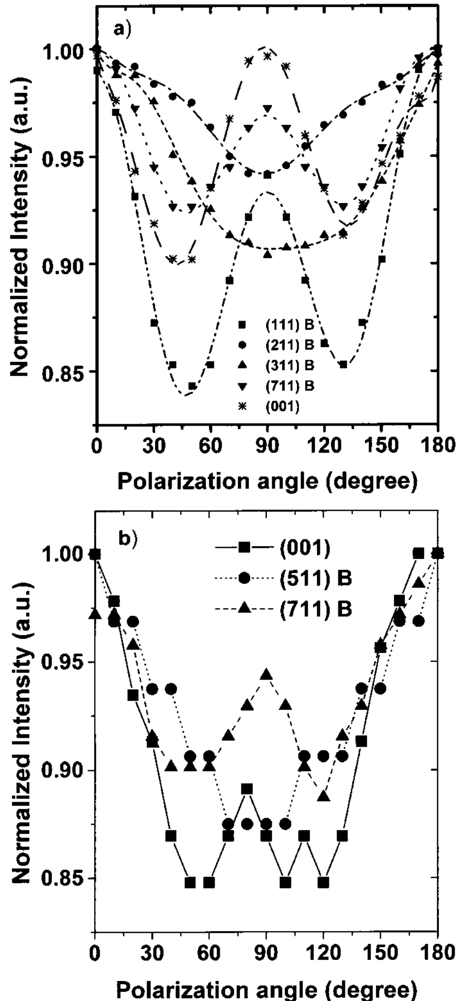

Figure 7. Angular dependence of normalized PL intensity for (a) InGaAs- and (b) InAs-quantum dots on differently orientated samples. (Taken from Ref. [28].).

IV. Vertically stacked self-assembled InGaAs QDs study

Recently, it has been shown that InAs-induced strain fields influence the adatom migration during subsequent GaAs structure layer growth[30]. Q. Xie et al.[31] have presented evidence for vertical alignment of coherent quantum dot islands separated by GaAs spacer layers along growth direction as a consequence of the strain fields created by the lower set of islands, a vertical alignment obtained on GaAs(001) substrates. On the other hand, growth of such structures on GaAs high-index surfaces has hardly been studied.

To investigate the influence of island induced stress field, we performed experiments with samples where the spacer layer thickness (d) varied. The initial set of islands, corresponding to 6 ML $In_{0.5}Ga_{0.5}As$ deposition, was grown at a rate of 0.11 nm/s on GaAs (001) and (311)A/B substrates at 500 °C. These islands were then covered with a GaAs layer (spacer). Afterwards, a second set of $In_{0.5}Ga_{0.5}As$ islands were formed under conditions identical to those of the first case. This combination of 6 ML $In_{0.5}Ga_{0.5}As$ and GaAs spacer layer was repeated 10 times. Details of growth were described previously[32]. Grown structures were studied by PL measurements under similar circumstances to the ones specified in section III.

IV.1 PL- and polarization-measurements

We have shown in Ref. [32] that the spacer layer plays an important role in the PL characteristic. Spectrum for the sample with a 6 nm spacer layer is shown in Fig. 8. The PL emission peak C is at lower energy when compared with the emission of a single set of islands for same spacer layer thickness, a difference probably due to coupling between the electronic states of islands, leading to a splitting of the states and a lowering of the ground state energy[33] Such a phenomenon becomes more probable when the islands are aligned closely enough. The Fig. 8 inset exhibits PL temperature dependence for the 6 nm spacer sample and shows

that at 100 K only peak C persists. This dependence suggests as much the lack of relation between peaks A-B and quantum dots, as their presumable relation to emission from coupled wetting layers. Peak signal C is assigned to vertically aligned islanding layers.

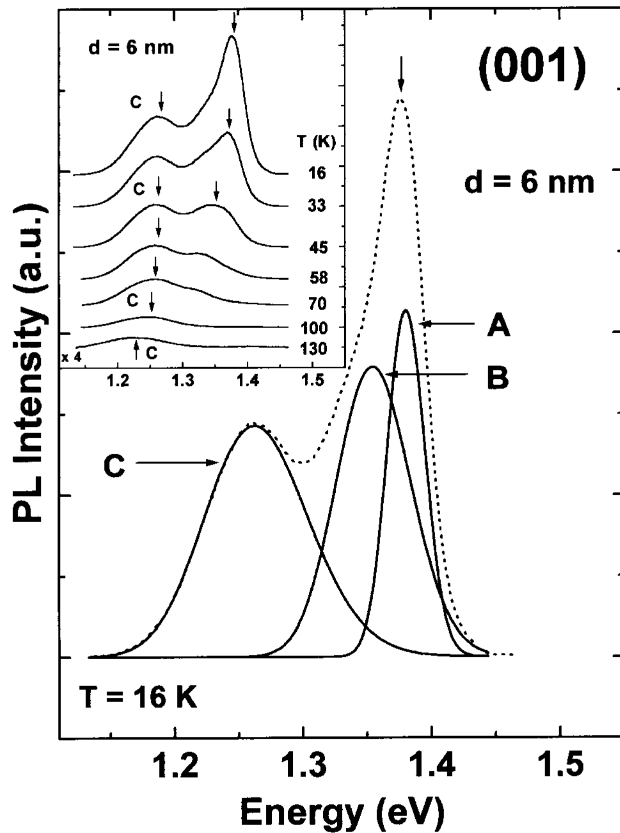

Figure 8. PL spectra (dotted line) of (001) plane for 6 nm spacer.

For the 10 nm spacer layer we believe that two kinds of quantum dots with different degrees of confinement are present on (001) plane (see Fig. 9). In Ref. [34], a broad high energy shoulder was also observed for vertically aligned InAs islands with 7.5 nm spacer. This shoulder was attributed to isolated, or only partially aligned, islands where coupling was either not present or was somewhat diminished. In our sample of 10 nm spacer, the (311)B orientation has the same form and temperature dependence as the (001) (see Fig. 10). We suppose this is due to the fact that (311)B orientation has similar surface properties as (001)[35]. In contrast, (311)A plane exhibits a different PL characteristic[32].

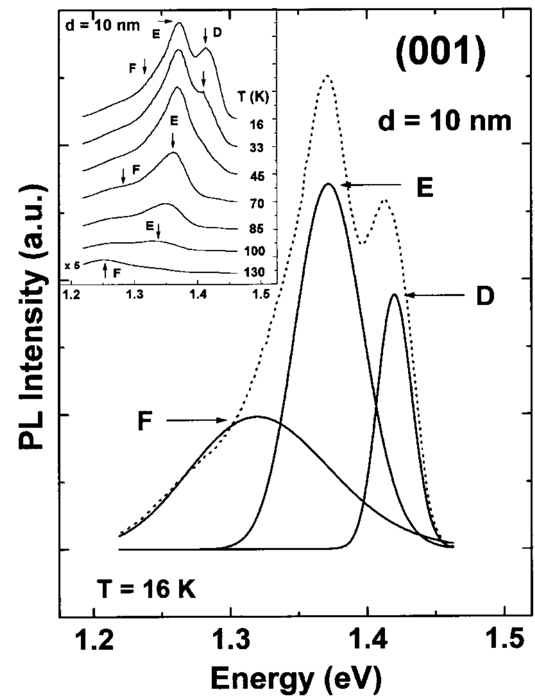

Figure 9. (001) PL temperature dependence of vertically stacked QDs for 10 nm spacer layer.

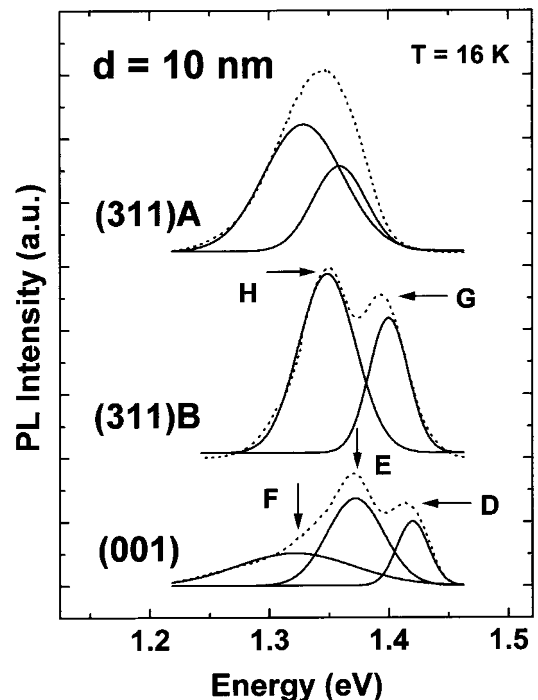

Figure 10. PL spectra (dotted lines) of vertical aligned self-assembled InGaAs QDs for 10 nm spacer layer for (001) and (311)A/B surfaces.

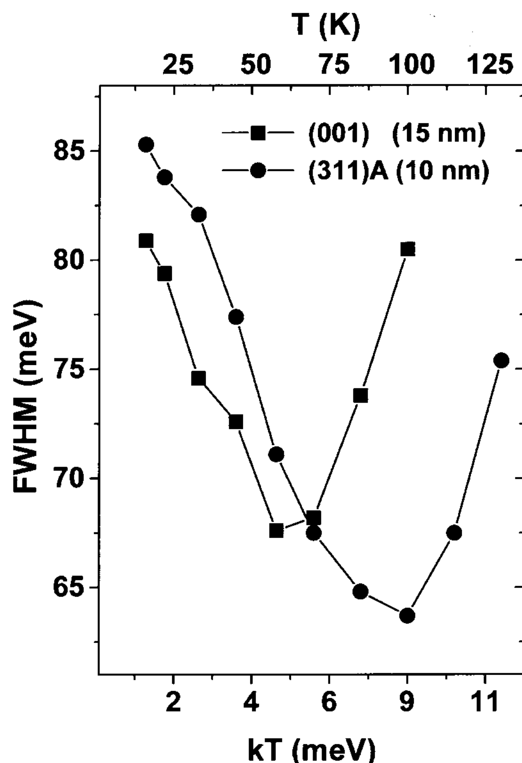

Figure 11. PL FWHM temperature dependence of (001) (square) (d=15 nm) and (311)A (circle) (d=10 nm) samples.

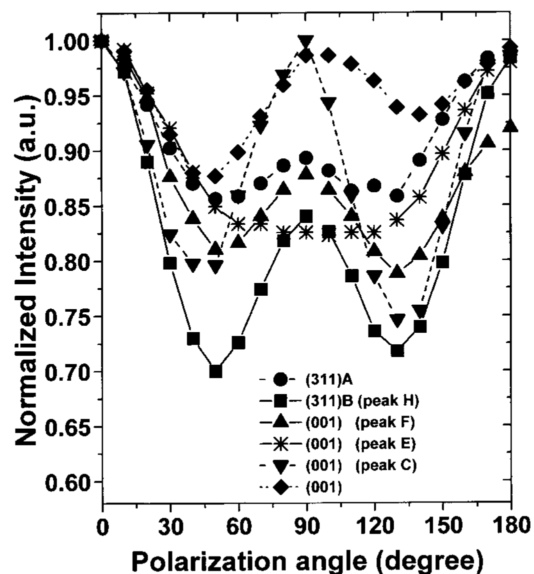

Figure 12. Angular dependence of normalized PL intensity for d = 15 nm (diamond (001)), d = 10 nm (square (311)B, circle (311)A, star and up triangle (001)) and d = 6 nm (down triangle (001)) samples.

Fig. 11 also shows an unexpected effect on PL FWHM as a function of temperature for (001) (15 nm) and (311)A (10 nm) orientations. On such surfaces, the unusual decrease of FWHM was also detected for the Gaussian- shaped emissions from 16 K to 58 K for (311)A and to 100 K for (100) plane, respectively.

Investigations of probable structural anisotropy of vertically stacked QDs, by means of PL polarization measurements, were also carried out. The angular dependence of normalized PL peak intensity for all samples is exhibited in Fig. 12, showing strong polarization effects. Maximum intensity, which has also been detected as described in section 3.3, occurs when polarization is parallel to crystallographic direction $[\bar{2}33]$ for (311) A/B and $[1\bar{1}0]$ for (001) plane, respectively. Based on these results, we also suppose that vertically aligned QDs grown on (311)A/B and (001) surfaces maintain the well-developed microfacet configuration.

V. Conclusions

The optical properties of self-assembled $In_{0.5}Ga_{0.5}As$ and InAs QDs grown by MBE on high-index GaAs surfaces have been investigated by means of PL measurements. Results reveal strong dependence of QD peak intensity, energy position and FWHM on substrate orientation. No InAs-QD formation was detected on (711)A and (511)A surfaces. For these surfaces an unexpected peak possibly related to a two dimensional layer, was observed. The results suggest that another growth mechanism predominated in the A planes as a result of stress relaxation. Our results also show an unusual decrease of PL FWHM with temperature for InAs QDs, as well as for vertically stacked QDs, suggesting suppression of non-predominant sizes and persistence of predominant ones. We believe that this unusual temperature dependence is a typical characteristic of self-assembled InAs QDs. All samples exhibit strong polarization dependence due to QD structural anisotropy. We have also observed that spacer layer and surface orientation play an important role in formation of self-stacked QD islands.

Acknowledgments

The authors would like to acknowledge Dr. F.E.G.

Guimarães, M. Sci. H. Arakaki and C.A. de Souza for their technical assistance. The financial support of CNPq and FAPESP is also gratefully acknowledged.

References

1. Y. Arakawa and H. Sasaki, Appl. Phys. Lett. **40**, 939 (1982).
2. G. W. Bryant, Phys. Rev. B**37**, 8763 (1988).
3. M. Asada, Y. Miyamoto and Y. Suematsu, IEEE J. Quantum Electr. **QE-22** 1915 (1986).
4. V. M. Ustinov, A. Yu. Egorov, A. E. Zhukov, N. N. Ledentsov, M. V. Maksimov, A. F. Tsatsul'nikov, S. V. Zaitsev, Yu. Gordeev, A. O. Kosogov, P. S. Kop'ev, D. Bimberg and Zh. I. Alferov, J. Cryst. Growth (1997) (accepted).
5. R. Mirin, J. Bowers and A. Gossard, J. Cryst. Growth (1997) (accepted).
6. K. Eberl, A. Kurtenbach, M. Zundel, J. Y. Phillipp, A. Moritz and A. Hangleiter, J. Cryst. Growth (1997) (accepted).
7. For a recent overview: A. Madhukar, Thin Solid Films **231**, 8 (1993).
8. J. A. Lebens, C. S. Tsai, K. J. Vahala and J. F. Kuech, Appl. Phys. Lett. **56,** 2642 (1990).
9. R. Notzel, N. N. Ledentsov, L. Daweritz, K. Ploog and M. Hohenstein, Phys. Rev. B **45**, 3507 (1993).
10. L. Goldstein, F. Glas, J. Y. Marzin, M. N. Charasse and G. Le Roux, Appl. Phys. Lett. **47**, 1099 (1985).
11. D. J. Eaglesham and M. Cerullo, Phys. Rev. Lett. **64**, 1943 (1990).
12. C. W. Synder, B. G. Orr, D. Kessler and L. M. Sander, Phys. Rev. Lett. **66**, 3032 (1990).
13. S. Guha, A. Madhukar and K. C. Rajkumar, Appl. Phys. Lett. **57**, 2110 (1990).
14. D. Leonard, K. Krishnamurhy, C. M. Reaves, S. P. Denbaars and P. M. Petroff, Appl. Phys. Lett. **63**, 3203 (1993).
15. A. Madhukar, Q. Xie, P. Chen and A. Kinkar, Appl. Phys. Lett. **64**, 2727 (1994).
16. R. Nötzel, J. Temmyo and T. Tamamura, Nature **369**, 131 (1994).
17. R. Nötzel, T. Fukui, H. Hasegawa, J. Temmyo and T. Tamamura, Appl. Phys. Lett. **65**, 2854 (1994).
18. R. C. Sangster, in: Compound Semiconductors, Ed. by R. K. Willardson and H. L. Goering (Reinhold, London, 1962), vol. 1, p. 241.
19. F. J. Grunthaner, M. Y. Yen, R. Fernandez, A. Madhukar and B. F. Lewis, Appl. Phys. Lett. **46**, 983 (1985).
20. R. Nötzel, L. Daweritz and K. Ploog, Phys. Rev. B **46**, 4736 (1992).
21. D. I. Lubyshev, P. P. González-Borrero, E. Marega Jr., E. Petitprez, N. La Scala Jr. and P. Basmaji, Appl. Phys. Lett.**68,** 205 (1996).
22. P. P. González-Borrero, D. I. Lubyshev, E. Marega Jr., E. Petitprez and P. Basmaji, J. Cryst. Growth **169**, 424 (1996).
23. G. Wang, S. Fafard, D. Leonard, J. E. Bowers, J. L. Merz and P. M. Petroff, Appl. Phys. Lett. **64**, 2815 (1994).
24. I. W. Tao, C. Schwartz and W. I. Wang, J. Vac. Sci. Technol. B **10**, 838 (1992).
25. P. P. González-Borrero, E. Marega Jr., D. I. Lubyshev, E. Petitprez and P. Basmaji, Superlatt. and Microstruct. **22** (accepted).
26. Z.Y. Xu, Z.D. Lu, X.P. Yang, Z.L. Yuan, B.Z. Zheng, J.Z. Xu, W. Zhang, W. K. Ge, Y. Wang, J. Wang and L.L. Chang, Superlatt. and Microstruct. **20** (accepted).
27. Y. Nabetani, T. Ishikawa, S. Noda and A. Sasaki, J. Appl. Phys. **76**, 347 (1994).
28. D. I. Lubyshev, P. P. González-Borrero, E. Marega Jr., E. Petitprez and P. Basmaji, J. Vac. Sci. Technol. B **14**, 2212 (1996).
29. P. P. González-Borrero, E. Marega Jr., D. I. Lubyshev, E. Petitprez and P. Basmaji, J. Cryst. Growth (accepted).
30. Q. Xie, P. Chen, and A. Madhukar, Appl. Phys. Lett. **65**, 2051 (1994).
31. Q. Xie, A. Madhukar, P. Chen and N. P. Kobayashi, Phys. Rev. Lett. **75**, 2542 (1995).
32. P. P. González-Borrero, D. I. Lubyshev, E. Marega Jr., E. Petitprez and P. Basmaji, Superlatt. and Microstruct. (accepted).
33. Q. Xie, N. P. Kobayashi, T. R. Ramachandran, A. Kalburge, P. Chen and A. Madhukar, J. Vac. Sci. Technol. B **14**, 2203 (1996).
34. G. S. Solomon, J. A. Trezza, A. F. Marshall and J. S. Harris Jr., J. Vac. Sci. Technol. B **14**, 2208 (1996).
35. F. Briones and A. Ruiz, J. Cryst. Growth **111**, 194 (1991).